Eddy Effects in the General Circulation, Spanning Mean Currents, Mesoscale Eddies, and Topographic Generation, Including Submesoscale Nests

Alexander F. Shchepetkin (PI)
James C. McWilliams and Maarten J. Molemaker (co-PIs)
Department of Atmospheric and Oceanic Sciences
University of California, Los Angeles, CA 90095-1565
phone:(310)206-9381 fax:(310)206-5219 email:alex@atmos.ucla.edu

N00014-12-1-0939
http://www.atmos.ucla.edu/roms/

LONG-TERM GOALS

Development of Regional Oceanic Modeling System (ROMS) with emphasis on the ability to simulate realistic, highly-turbulent flows in both basin- and local regional scales, at resolutions sufficient to capture submesoscale phenomena; analysis and understanding the underlying physical processes; improving parameterizations of unresolved processes, applicable numerical algorithms, relevant computer-science techniques needed for efficient parallel code adapted for modern computing environment.

OBJECTIVES

The scientific question is how the eddies control the currents by the eddy-induced momentum and buoyancy fluxes, turbulent mixing, and their bottom form stress (pressure force) and bottom boundary layers – all the aspects associated with turbulent flows over steep topography in the presence of stratification. This is done in the context of western boundary currents, the Gulf Stream and the Kuroshio, as well as the western Pacific (Solomon Sea). The intend is obtain realistically accurate separation and the subsequent path of the Gulf Stream, the Kuroshio path from Taiwan to Japan with subsequent separation, as well as, provide analysis of modeling sensitivities to input parameters and forcing, and, wherever possible, to understand and give a physical explanation of the underlying mechanisms. This involves validation against real-world data in cooperation with William S. Kessler and Hristina Hristova from PMEL (Solomon Sea), and Satoshi Miarai, Taichi Sakagami from Okinawa Institute of Science and Technology (Kuroshio).

APPROACH

The primary method is to obtain numerical solution on sets of progressively refined grids, starting with basin-wide eddy permitting resolutions (although substantially finer than that used in climate modeling), and downscaling it to $\Delta x \sim 1km$ or less which enables adequate resolution of mesoscale and submesoscale eddies generated by instability and bottom topography effects. This is accompanied by development of modeling codes, numerical methods, and the associated pre- and post-processing infrastructure, analysis, visualization that allows prioritizing the tasks directly necessary for achieving the objectives stated above, but, at the same time, traditionally maintaining the 3-way balance among physical applications (including introducing new submodels), numerical methods, and computer science that has been established throughout ROMS development history.

Report Documentation Page

Form Approved
OMB No. 0704-0188

1. REPORT DATE	2. REPORT TYPE	3. DATES COVERED
30 SEP 2013		**00-00-2013 to 00-00-2013**

4. TITLE AND SUBTITLE	5a. CONTRACT NUMBER
Eddy Effects in the General Circulation, Spanning Mean Currents, Mesoscale Eddies, and Topographic Generation, Including Submesoscale Nests	5b. GRANT NUMBER
	5c. PROGRAM ELEMENT NUMBER
6. AUTHOR(S)	5d. PROJECT NUMBER
	5e. TASK NUMBER
	5f. WORK UNIT NUMBER
7. PERFORMING ORGANIZATION NAME(S) AND ADDRESS(ES) **University of California Los Angeles,Department of Atmospheric & Oceanic Sciences,Los Angeles,CA,90095**	8. PERFORMING ORGANIZATION REPORT NUMBER
9. SPONSORING/MONITORING AGENCY NAME(S) AND ADDRESS(ES)	10. SPONSOR/MONITOR'S ACRONYM(S)
	11. SPONSOR/MONITOR'S REPORT NUMBER(S)

12. DISTRIBUTION/AVAILABILITY STATEMENT
Approved for public release; distribution unlimited

13. SUPPLEMENTARY NOTES

14. ABSTRACT

15. SUBJECT TERMS

16. SECURITY CLASSIFICATION OF:			17. LIMITATION OF ABSTRACT	18. NUMBER OF PAGES	19a. NAME OF RESPONSIBLE PERSON
a. REPORT	b. ABSTRACT	c. THIS PAGE			
unclassified	**unclassified**	**unclassified**	**Same as Report (SAR)**	**15**	

Additionally, we design idealized, process-study-oriented simulations with the intent of understanding of physical phenomena, and as control tests for algorithm verification.

WORK COMPLETED

During the last year we worked on decadal Pacific and Atlantic circulations, the Kuroshio, and the Gulf Stream; mesoscale eddy buoyancy fluxes; submesoscale surface fronts, filaments, and eddies; topographic current separation, form stress, and submesoscale vortex generation; Our work on isoneutral diffusion for tracers is now published, Lemarié, *et al.*(2012a,b), however most recently we have revisited the relevant parts of the code with the intent of reducing its computational cost, and for better integration with the rest of the model. On the new algorithmic direction we implemented adaptively implicit vertical advection to alleviate the associated CFL limitations, which has been a growing impediment for high-resolution simulations, as well as for modeling tides. The code now utilizes dual (shared- and distributed-memory) parallelization (implemented via Open MP and MPI, respectively, with an option to use both at the same time) based on subdomain decomposition for both with two-level hierarchy. We also made an effort to parallelize pre-processing software tools wherever justified by their computational cost. A substantial effort on analysis and visualization techniques was performed by Jonathan Gula that involves transition from Matlab to Python-based software and graphics.

RESULTS

We present a few highlights for this project. The publications list (papers from 2012 up to ones likely to be submitted in 2013) provides a view of the finalized results across all our ONR projects.

Eddy buoyancy fluxes: It is now widely understood that mesoscale eddy fluxes play a central role in the oceanic general circulation, requiring that they either be parameterized (as in most climate simulations) or adequately resolved with grid scales of $\Delta x = 10$ km or smaller. Nevertheless, their spatial heterogeneity and long time scales of dynamical equilibration make them difficult to measure accurately and challenging to interpret in models. A dynamical interpretation is made of the mesoscale eddy buoyancy fluxes in the Eastern Boundary Currents of California and Peru-Chile, based on regional equilibrium ROMS simulations. The eddy fluxes are primarily shoreward and upward across a swath several hundred km wide in the upper ocean (Fig. 1); as such they serve to balance mean air-sea heating and cooling by coastal upwelling. In the stratified interior the eddy fluxes are consistent with the adiabatic/isopypcnal hypothesis associated with a mean, eddy-induced velocity advecting mean buoyancy and tracers in a materially conservative way that extracts potential energy from the mean flow. Furthermore, with a suitable gauge choice, the horizontal fluxes are almost entirely aligned with the mean horizontal buoyancy gradient, consistent with the advective parameterization scheme of Gent and McWilliams (*JPO*, 1990). The associated diffusivity is surface-intensified, matching the vertical stratification profile below the boundary layer. The fluxes span the across-shore band of high eddy energy (hundreds of km wide), but their along-shore structure is unresolved due to statistical sampling limitations. In the surface layer the eddy flux is significantly diabatic with a shallow eddy-induced (Lagrangian) circulation cell and down-gradient lateral diapycnal flux. These effects are summarized in Fig. 2. The dominant eddy generation process is baroclinic instability, but there are significant regional differences between the different upwelling systems in the flux pattern and the associated κ profiles that are not consistent with simple baroclinic instability theory (Colas *et al.*, 2013a).

Dynamical balance of the Gulf Stream: Identifying the dynamics responsible for the Gulf Stream separation and control of its path has been a long-standing challenge in oceanography. The dynamical balance of the Gulf Stream is investigated using very high-resolution ROMS simulations highlighting the important role played by eddy-driven flows and the interactions with complex topography.

The bottom pressure torque, which derive from the twisting of the force that the bottom topography exert on the ocean, is the main ingredient enabling the return flow of the wind-driven transport in western boundary currents. The bottom pressure torque strongly reflects the regional topography as seen on Fig. 3. The planetary vorticity term, related to meridional transport of fluid, is balanced by the sum of the bottom pressure torque and the non-linear advective term in the barotropic vorticity balance equation. The non-linear advective term redistributes vorticity locally but spatially averages to zero for areas larger than $\approx 2^\circ \times 2^\circ$. Hence the bottom pressure torque is the term providing the overall positive input of vorticity, balancing the negative input by anticyclonic wind curl on the scale of the subtropical gyre. Differences between the two bottom panels of Fig. 3, especially in the Charleston Bump region, are due to the contribution of the bottom stress curl. Fig. 4 shows how the Gulf Stream path is directly linked to the Bottom Pressure Torque, and its related eddy-driven abyssal circulation, through vertical fluxes of vorticity.

Energy conversions at the topographic features, especially the Charleston Bump and at the separation point after Cape Hatteras, show that they are triggers for instability processes and baroclinic-barotropic energy conversions. The eddy potential to eddy kinetic energy ($\overline{w'b'}$, Fig. 5) shows a strong baroclinic conversion right after separation and near the Charleston Bump, with very small or negative signals in-between. The mean kinetic to eddy kinetic energy due to the horizontal and vertical Reynolds stresses ($K_m K_e = HRS + VRS$, Fig. 5) also shows a barotropic conversion in the same places. The topographic constraint has a stabilizing effect on the flow upstream from the Charleston Bump. This constraint is reduced as the stream is deflected seaward by the Bump where the topography is deeper and a relatively large conversion of mean energy to eddy energy can happen. The topographic constaint is renewed between the Bump and Cape Hatteras while the Gulf Stream flows northeastward and requires that some eddy energy be converted back to mean energy. The strongest eddy generation happens after separation of the Gulf Stream due to the increased transport and the confluence of the flow which acts to sharpen the cross frontal gradients of the mean flow.

Adaptively-implicit vertical advection for momentum and tracers: As any oceanic model with an Eulerian vertical coordinate, ROMS is subject to the CFL limitation associated with vertical advection. When the goal is to produce a simulation with horizontal resolution less than a few km this limitation gradually becomes the most restrictive one (depending on the topographic features and/or whether or not the tides are part of the simulation). For sub-$1km$ grids it becomes so dominant that the imposed time step limitation is several times smaller than that due to horizontal advection and/or internal wave phase speeds. Detailed investigation of the associated "hot spots" (characteristic locations on the model grid where numerical instability of the explicit code occurs first) reveals large vertical CFL always occur near topographic features, where buoyancy stratification is weak or vanishing, but not necessarily in the shallowest areas where vertical grid spacing is the smallest due to topography-following coordinate.

While implicit advection schemes offer a relief from CFL limitation, their drawbacks are well known: unavoidable and potentially large dispersive errors increasing with CFL, and depending on the detail of time and space discretization, large numerical viscosity as well (*cf.,* Shchepetkin & McWilliams, 2008). In contrast, the explicit vertical advection schemes of ROMS are designed to be

high order in space (4th-centered or compact based parabolic spline fits), which makes it not feasible to design an implicit version of comparable accuracy.

To overcome the dilemma we pursue an adaptive approach where the scheme remains explicit (as in the original code) everywhere except where/when local vertical velocities exceed a threshold close to (but below) the explicit stability limit. Once this happens, a gradual transition toward an implicit scheme begins via Courant-number-dependent weighting algorithm. As we are not aware of any prototype of such approach published in the literature, we present a few detail here. Vertical advection fluxes for the tracer or velocity fields are discretized in such a way that their computation involve the advected field at the new time step, q_k^{n+1} which is yet unknown,

$$FC_{k+1/2} = W_{k+1/2} \cdot \mathscr{Q}\left(q_k^{n+1}, q_{k\pm1}^{n+1}, q_k^{n+1/2}, q_{k\pm1}^{n+1/2}, ...\right) . \tag{1}$$

This can be rearranged by splitting vertical velocity into two parts,

$$W_{k+1/2} = W_{k+1/2}^{(e)} + W_{k+1/2}^{(i)}, \qquad \forall k = 0, 1, ..., N \tag{2}$$

where $W_{k+1/2}^{(i)}$ is used to compute terms involving $q_k^{n+1}, q_{k\pm1}^{n+1}$ only (*i.e.,* implicit part), while $W_{k+1/2}^{(e)}$ for the remaining $q_k^{n+1/2}, q_{k\pm1}^{n+1/2}, ...$ (half-integer time index $n + 1/2$ means that these are provisional values from ROMS predictor-corrector stepping, Sec. 4 in Shchepetkin & McWilliams, 2005). Then, $W^{(e)}$-terms are computed via standard algorithm within the r.h.s., while $W^{(i)}$-terms are integrated into the vertically implicit operator. Assuming upstream treatment of the implicit part,

$$FC_{k+1/2}^{(i)} = W_{k+1/2}^{(i)} \cdot \begin{cases} q_{k-1}^{n+1}, & \text{if} \quad W_{k+1/2}^{(i)} > 0 \\ q_k^{n+1}, & \text{if} \quad W_{k+1/2}^{(i)} < 0 \end{cases} \tag{3}$$

the combined implicit advection-diffusion system becomes

$k = N$, uppermost grid box,

$$\begin{aligned} H_N^{n+1} q_N^{n+1} = H_N^n q_N^n + \Delta t \cdot \mathrm{rhs}'_N + \Delta t \cdot SRFRC - \Delta t A_{N-1/2} \frac{q_N^{n+1} - q_{N-1}^{n+1}}{\Delta z_{N-1/2}} \\ + \Delta t \left[\max\left(W_{N-1/2}^{(i)}, 0\right) q_{N-1}^{n+1} + \min\left(W_{N-1/2}^{(i)}, 0\right) q_N^{n+1} \right] \end{aligned} \tag{4}$$

$k = 2, ..., N-1$

$$\begin{aligned} H_k^{n+1} q_k^{n+1} = H_k^n q_k^n + \Delta t \cdot \mathrm{rhs}'_k + \Delta t A_{k+1/2} \frac{q_{k+1}^{n+1} - q_k^{n+1}}{\Delta z_{k+1/2}} - \Delta t \left[\max\left(W_{k+1/2}^{(i)}, 0\right) q_k^{n+1} \right. \\ \left. + \min\left(W_{k+1/2}^{(i)}, 0\right) q_{k+1}^{n+1} \right] \\ - \Delta t A_{k-1/2} \frac{q_k^{n+1} - q_{k-1}^{n+1}}{\Delta z_{k-1/2}} + \Delta t \left[\max\left(W_{k-1/2}^{(i)}, 0\right) q_{k-1}^{n+1} \right. \\ \left. + \min\left(W_{k-1/2}^{(i)}, 0\right) q_k^{n+1} \right] \end{aligned} \tag{5}$$

$k = 1$, bottom grid box,

$$\begin{aligned} H_1^{n+1} q_1^{n+1} = H_1^n q_1^n + \Delta t \cdot \mathrm{rhs}'_1 + \Delta t A_{3/2} \frac{q_2^{n+1} - q_1^{n+1}}{\Delta z_{3/2}} - \Delta t \left[\max\left(W_{3/2}^{(i)}, 0\right) q_1^{n+1} \right. \\ \left. + \min\left(W_{3/2}^{(i)}, 0\right) q_2^{n+1} \right] \end{aligned} \tag{6}$$

where the prime in rhs'_k means that the usual r.h.s. computed by ROMS code for the corresponding equations, except the replacement $W_{k+1/2} \to W^{(e)}_{k+1/2}$; $A_{k+1/2}$ is vertical viscosity/diffusion coefficient (including the stabilization terms, Sec. 3 from Lemarié, *et al.*(2012b), in the case when isoneutral lateral diffusion is used). The above system takes into account kinematic b.c. at surface and bottom, $W_{N+1/2} = W_{1/2} = 0$, bottom no-flux b.c. for tracers (Eq. (6) for the momentum equation contains an extra term associated with bottom drag, which also treated implicitly). As in the original ROMS code, the new algorithm has simultaneous conservation and constancy preservation properties for tracers, despite the fact that grid box heights change due to changing free surface, $H^{n+1}_k \neq H^n_k$.

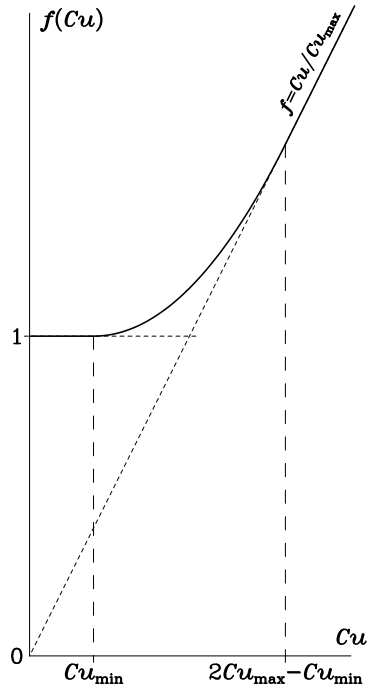

The splitting in (2) works as follows: At first the vertical velocity $W_{k+1/2}$ is computed the standard way, and, in addition to that, also computed is the finite-volume Courant number Cu_k (defined at every grid box H_k as the sum of fluxes outgoing from H_k, normalized by the time step size Δt and grid-box volume). The explicit part is then computed as

$$W^{(e)}_{k+1/2} = \frac{W_{k+1/2}}{f(C^*)}, \qquad \begin{cases} C^* = Cu_k & \text{if} \quad W_{k+1/2} > 0 \\ C^* = Cu_{k+1} & \text{if} \quad W_{k+1/2} < 0 \end{cases}$$

while the implicit is the remainder,

$$W^{(i)}_{k+1/2} = W_{k+1/2} - W^{(e)}_{k+1/2}\,.$$

The limiting function $f = f(Cu)$ is shown on the left, and consists of three segments: constant, parabolic, and linear, smoothly matched to each other. The two parameters $Cu_{\min}$ and $Cu_{\max}$ control the threshold below which the algorithm is fully explicit as is the original ROMS code, and the maximum allowed Courant number for the explicit part. The practical values we select in our computations are $Cu_{\min} = 0.2$ and $Cu_{\max} = 0.5$, which is based on consideration of numerical stability, and accuracy as well.

The motivation for using upstream discretization for the implicit part comes from the fact that while it is diffusive, it is monotonic and has smaller numerical dispersion in its truncation term than the centered scheme (due to avoidance of spatial averaging). This leads to a well posed, diagonally dominant discrete system. This choice is further justified by the observation that in practical model solutions large vertical velocities occur only in places with vanishing (or even unstable) stratification and, consequently, already large mixing set by the vertical parameterization scheme.

To demonstrate the viability of the proposed algorithm we present test results from gravitational adjustment "lock-exchange" problem, Fig. 6. This problem is known for generating sharp fronts with the resulting vertical velocities playing the dominant factor in CFL stability. The adaptively implicit algorithm allows dramatic increase of the allowed time step. For the smallest settings of Δt, adaptive and explicit solutions are identical (which is expected), while for the largest Δt adaptive solution becomes more similar to fully implicit (backward Euler in time, upstream in space). Also note the progressive delay in the front propagation for the largest Δt – neither adaptive, nor fully implicit scheme is expected to be accurate at this regime ($\Delta t = 240...510s$), but still adaptive shows slightly less delay and less mixing.

TRANSITIONS

ROMS modeling code and the associated supporting software are generally available as open source. We also made available some of our solutions for the analysis by a third party.

RELATED PROJECTS

Wave-current interaction (in cooperation with Yusuke Uchiyama, University of Kobe, Japan); Biogeochemistry modeling (in cooperation with Curtis Deutsch, Jun-Hong Liang, and Hartmut Frenzel, from University of Washington)

REFERENCES

Benjamin, T.B., 1968. Gravity currents and related phenomena. *J. Fluid Mech.*, **31**, 209-248.

Gent, P. R. and J. C. Mcwilliams, 1990: Isopycnal mixing in ocean circulation models. *J. Phys. Oceanogr.*, **20**, 150-155, doi:10.1175/1520-0485(1990)020<0150:IMIOCM>2.0.CO;2.

Haidvogel, D. B. and A. Beckmann, 1999. Numerical Ocean Circulation Modeling. *Imperial College Press*, 318 pp.

Ilicak, M., A. J. Adcroft, S. M. Griffies, and R. W. Hallberg, 2012: Spurious dianeutral mixing and the role of momentum closure. *Ocean Modeling*, **45-46**, 37-58, doi:10.1016/j.ocemod.2011.10.003

Shchepetkin, A. F. and J. C. McWilliams, 2005: The regional oceanic modeling system (ROMS): A split-explicit, free-surface, topography-following-coordinate oceanic model. *Ocean Modeling* **9**/4, pp. 347-404, doi:10.1016/j.ocemod.2004.08.002.

Shchepetkin, A. F. and J. C. McWilliams, 2008: Computational kernel algorithms for fine-scale, multi-process, long-term oceanic simulations. In: *Handbook of Numerical Analysis, Vol. XIV: Computational Methods for the Ocean and the Atmosphere*, P. G. Ciarlet, editor, R. Temam & J. Tribbia, guest eds., *Elsevier Science*, pp. 121-183, doi:10.1016/S1570-8659(08)01202-0

PUBLICATIONS

Bracco, A., J. D Neelin, H. Luo, J. C. McWilliams, and J. E. Meyerson, 2013: High dimensional decision dilemmas in climate models. *Geosci. Model Dev.*, **6**, 2731-2767, doi:10.5194/gmdd-6-2731-2013.

Buijsman, M.C., Y. Uchiyama, J. C. McWilliams, and C. R. Hill-Lindsay, 2012: Modeling semidiurnal internal tide variability in the Southern California Bight. *J. Phys. Oceanogr.* **42**, 62-77, doi:10.1175/2011JPO4597.1

Chekroun, M. D., J. D. Neelin, D. Kondrashov, J. C. McWilliams, and M. Ghil, 2013: Rough parameter dependence in climate models: The role of Ruelle-Pollicott resonances. *Proc. Nat. Acad. Sci.*, submitted.

Colas, F., J.C. McWilliams, X. Capet, and J. Kurian, 2012: Heat balance and eddies in the Peru-Chile Current System. *Climate Dynamics* **39**, 509-529, doi:10.1007/s00382-011-1170-6.

Colas, F., X. Capet, J.C. McWilliams, and Z. Li, 2013a: Mesoscale eddy buoyancy flux and

eddy-induced circulation in eastern boundary currents. *J. Phys. Oceanogr.*, **43**, 1073-1095, doi:10.1175/JPO-D-11-0241.1.

Colas, F., X. Wang, X. Capet, Y. Chao, and J.C. McWilliams, 2013b: Untangling the roles of wind, run-off and tides in Prince William Sound. *Continen. Shelf Res.*, **63**, S79-S89, doi:10.1016/j.csr.2012.05.002.

Dong, C., X. Lin,, Y. Liu, F. Nencioli, Y. Chao, Y. Guan, T. Dickey, and J. C. McWilliams, 2012: Three-dimensional oceanic eddy analysis in the Southern California Bight from a numerical product. *J. Geophys. Res.*, **117**, C00H14, doi:10.1029/2011JC007354.

Farrara, J., Y. Chao, Z. Li, X. Wang, X. Jin, H. Zhang, P. Li, Q. Vu, P. Olsson, C. Schoch, M. Halverson, M. Moline, C. Ohlmann, M. Johnson, J. C. McWilliams, and F. Colas, 2013: A data-assimilative ocean forecasting system for the Prince William Sound and an evaluation of its performance during Sound Predictions 2009. *Continental Shelf Research*, **63**, S193-S208, doi:10.1016/j.csr.2012.11.008.

Gula. J., M. J. Molemaker, and J. C. McWilliams, 2013a: Mean dynamic balances in the Gulf Stream in high-resolution numerical simulations, *in preparation*.

Gula. J., M. J. Molemaker, and J. C. McWilliams, 2013b: Gulf Stream dynamics and frontal eddies along the Southeast U.S. continental shelf, *in preparation*.

Gula. J., M. J. Molemaker, and J. C. McWilliams, 2013c: Submesoscale cold filaments in the Gulf Stream, *in preparation*.

Gula. J., M. J. Molemaker, and J. C. McWilliams, 2013d: Submesoscale instabilities on the Gulf Stream north wall. *in preparation*.

Lemarié, F., J. Kurian, A.F. Shchepetkin, M.J. Molemaker, F. Colas, and J. C. McWilliams, 2012a: Are there inescapable issues prohibiting the use of terrain-following coordinates in climate models? *Ocean Modelling* **42**, 57-79, doi:10.1016/j.ocemod.2011.11.007.

Lemarié, F., L. Debreu, L., A.F. Shchepetkin, and J.C. McWilliams, 2012b: On the stability and accuracy of the harmonic and biharmonic adiabatic mixing operators in ocean models. *Ocean Modelling* **52-53**, 9-35, doi:10.1016/j.ocemod.2012.04.007.

Li, Z., Y. Chao, J. Farrara, and J. C. McWilliams, 2013: Impacts of distinct observations during the 2009 Prince William Sound field experiment: A data assimilation study. *Continental Shelf Research*, **63**, S209-S222, doi:10.1016/j.csr.2012.06.018

Li, Z., Y. Chao, J. McWilliams, K. Ide, and J. D. Farrara, 2012: A multi-scale three-dimensional variational data assimilation and its application to coastal oceans. *Q. J. Roy. Met. Soc.*, submitted.

Li, Z., Y. Chao, J.C. McWilliams, K. Ide, and J. Farrara, 2012: Experiments with a multi-scale data assimilation scheme. *Tellus Series A: Dynamic Meteorology and Oceanography*, submitted.

Liang, J.-H., J. C. McWilliams, P. P. Sullivan, and B. Baschek, 2012: Large Eddy Simulation of the bubbly ocean: Impacts of wave forcing and bubble buoyancy. *J. Geophys. Res.* **117**, C04002, doi:10.1029/2011JC007766.

Liang J.-H., J. C. McWilliams, J. Kurian, P. Wang, and F. Colas, 2012: Mesoscale variability in the

Northeastern Tropical Pacific: Forcing mechanisms and eddy properties. *J. Geophys. Res.* **117**, C07003, doi:10.1029/2012JC008008.

Liang, J.-H., C. Deutsch, J. C. McWilliams, B. Baschek, P. P. Sullivan, and D. Chiba, 2013: Parameterizing bubble-mediated air-sea gas exchange and its effect on ocean ventilation. *Glob. Biogeo. Cycles*, **27**, doi:10.1002/gbc.20080.

McWilliams, J. C., E. Huckle, J. Liang, and P. P. Sullivan, 2012: The wavy Ekman layer: Langmuir circulations, breakers, and Reynolds stress. *J. Phys. Oceanogr.*, **42**, 1793-1816, doi:10.1175/JPO-D-12-07.1.

McWilliams, J. C., and B. Fox-Kemper, 2013: Oceanic Wave-balanced surface fronts and filaments. *J. Fluid Mech.*, **730**, 464-490, doi:10.1017/jfm.2013.348.

McWilliams, J. C., E. Huckle, J. Liang, and P. P. Sullivan, 2013: Langmuir Turbulence in swell. *J. Phys. Oceanogr.*, submitted.

Mechoso, C. R., R. Wood, R. Weller, C. S. Bretherton, A. D. Clarke, H. Coe, C. Fairall, J. T. Farrar, G. Feingold, R. Garreaud, C. Grados, J. McWilliams, S. P. de Szoeke, S. E. Yuter, and P. Zuidema, 2013: Ocean-Cloud-Atmosphere-Land Interactions in the Southeastern Pacific: The VOCALS Program. *Bull. Amer. Met. Soc.*, doi:10.1175/BAMS-D-11-00246.1.

Menesguen, C., J. C. McWilliams, and M. J. Molemaker, 2012: An example of ageostrophic instability in a rotating stratified flow. *J. Fluid Mech.*, **711**, 599-619, doi:10.1017/jfm.2012.412.

Molemaker, M. J., J. C. McWilliams, and W. K. Dewar, 2013: Submesoscale instability and generation of mesoscale anticyclones near a separation of the California Undercurrent. *J. Phys. Oceanogr.*, submitted.

Molemaker, M. J., J. C. McWilliams, and W. K. Dewar, 2013: Centrifugal instability and mixing in the California Undercurrent. *J. Phys. Oceanogr.*, submitted.

Romero, L., Y. Uchiyama, J. C. Ohlmann, J. C. McWilliams, and D. A. Siegel, 2013: Simulations of nearshore particle-pair dispersion in Southern California *J. Phys. Oceanogr.*, **43**, 1862-1879, doi:10.1175/JPO-D-13-011.1.

Roullet, G., J. C. McWilliams, X. Capet, and M. J. Molemaker, 2012: Properties of equilibrium geostrophic turbulence with isopycnal outcropping. *J. Phys. Oceanogr.*, **42**, 18-38, doi:10.1175/JPO-D-11-09.1.

Shcherbina, A. Y., E. A. D'Asaro, C. M. Lee, J. M. Klymak, M. J. Molemaker, and J. C. McWilliams, 2013: Statistics of vertical vorticity, divergence, and strain in a developed submesoscale turbulence field. *Geophys. Res. Lett.*, **40**, doi:10.1002/grl.50919.

Sullivan, P. P., L. Romero, J. C. McWilliams, and W. K. Melville, 2012: Transient evolution of Langmuir Turbulence in ocean boundary layers driven by hurricane winds and waves. *J. Phys. Oceanogr.* **42**, 1959-1980, doi:10.1175/JPO-D-12-025.1.

Sullivan, P. P., J. C. McWilliams, and E. G. Patton, 2013: A high-Reynolds number Large Eddy Simulation model of the marine atmospheric boundary layer above a spectrum of moving waves, in preparation.

Uchiyama, Y., E. Idica, J. C. McWilliams, and K. Stolzenbach, 2013: Wastewater effluent dispersal in two Southern California Bays. *Cont. Shelf Res.*, submitted.

Wang, P., J. C. McWilliams, and Z. Kizner, 2012: Ageostrophic instability in rotating shallow water. *J. Fluid Mech.*, **712**, 327-353, doi:10.1017/jfm.2012.422.

Wang, P., J. C. McWilliams, and C. Ménesguen, 2013: Ageostrophic instability in rotating, stratified interior vertical shear flows. *J. Fluid Mech.*, submitted.

Wang, X., Y. Chao, H. Zhang, J. Farrara, Z. Li, X. Jin, K. Park, F. Colas, J. C. McWilliams, C. Paternostro. C.K. Shum, Y. Yi, C. Schoch, and P. Olsson, 2013: Modeling tides and their influence on the circulation in Prince William Sound, Alaska. *Continental Shelf Research*, **63**, S126-S137, doi:10.1016/j.csr.2012.08.016.

FIGURES

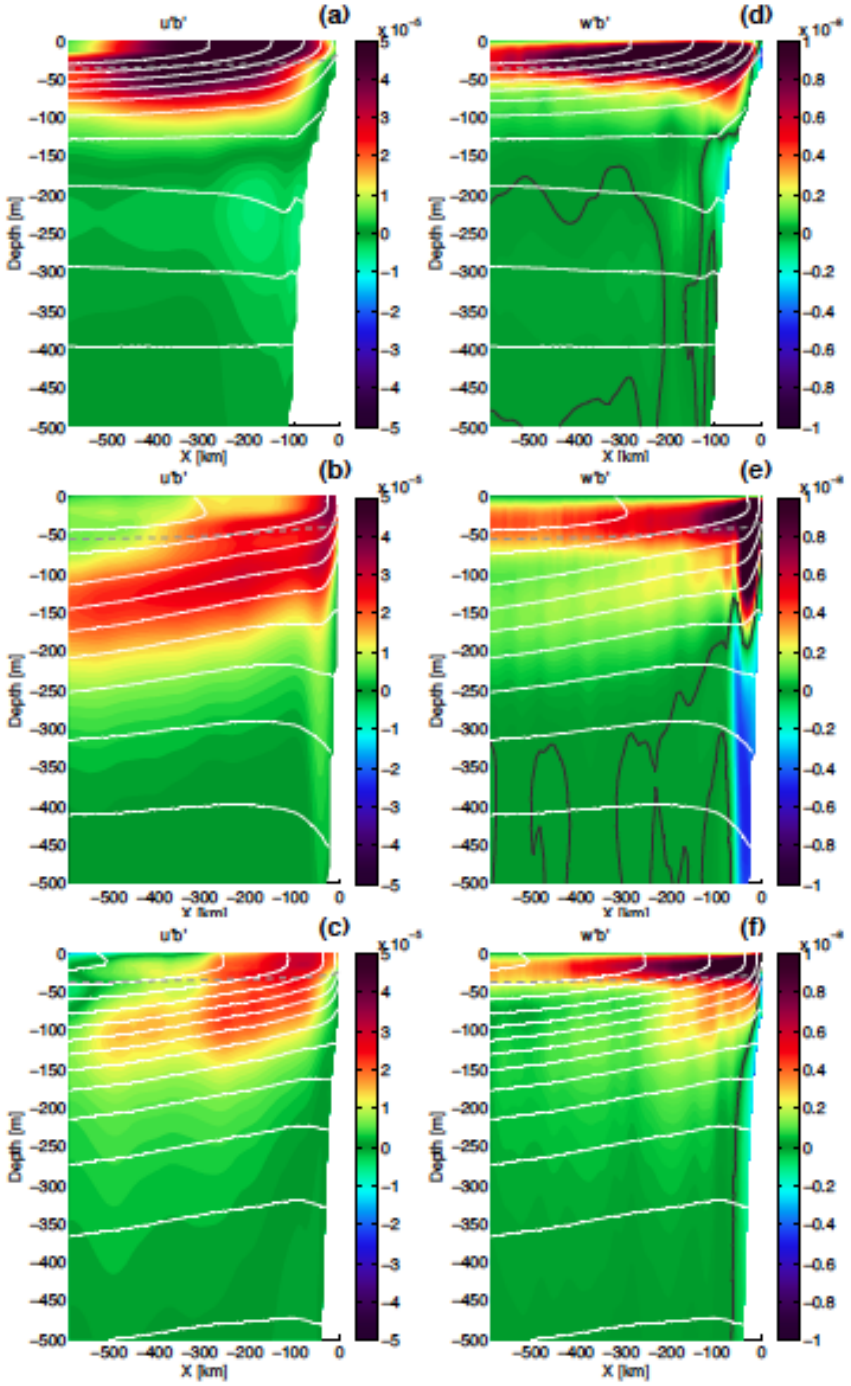

Figure 1: ***Annual and along-shore averages of across-shore (left) and vertical (right) eddy buoyancy flux [m^2 s^{-3}] for the Peru (top), Chile (middle), and California (bottom) current systems. White contours are the mean buoyancy field, and the gray dashed line is the boundary-layer depth diagnosed by the K-Profile Parameterization. Black contours are vertical flux $w'b' = 0$. The eddy flux patterns are generally shoreward in $u'b'$ and upward in $w'b'$, acting to balance the air-sea heating and mean upwelling circulations. While there is general qualitative similarity across the regions, there are noticeable regional differences in stratification and fluxes. (Colas et al., 2013a)***

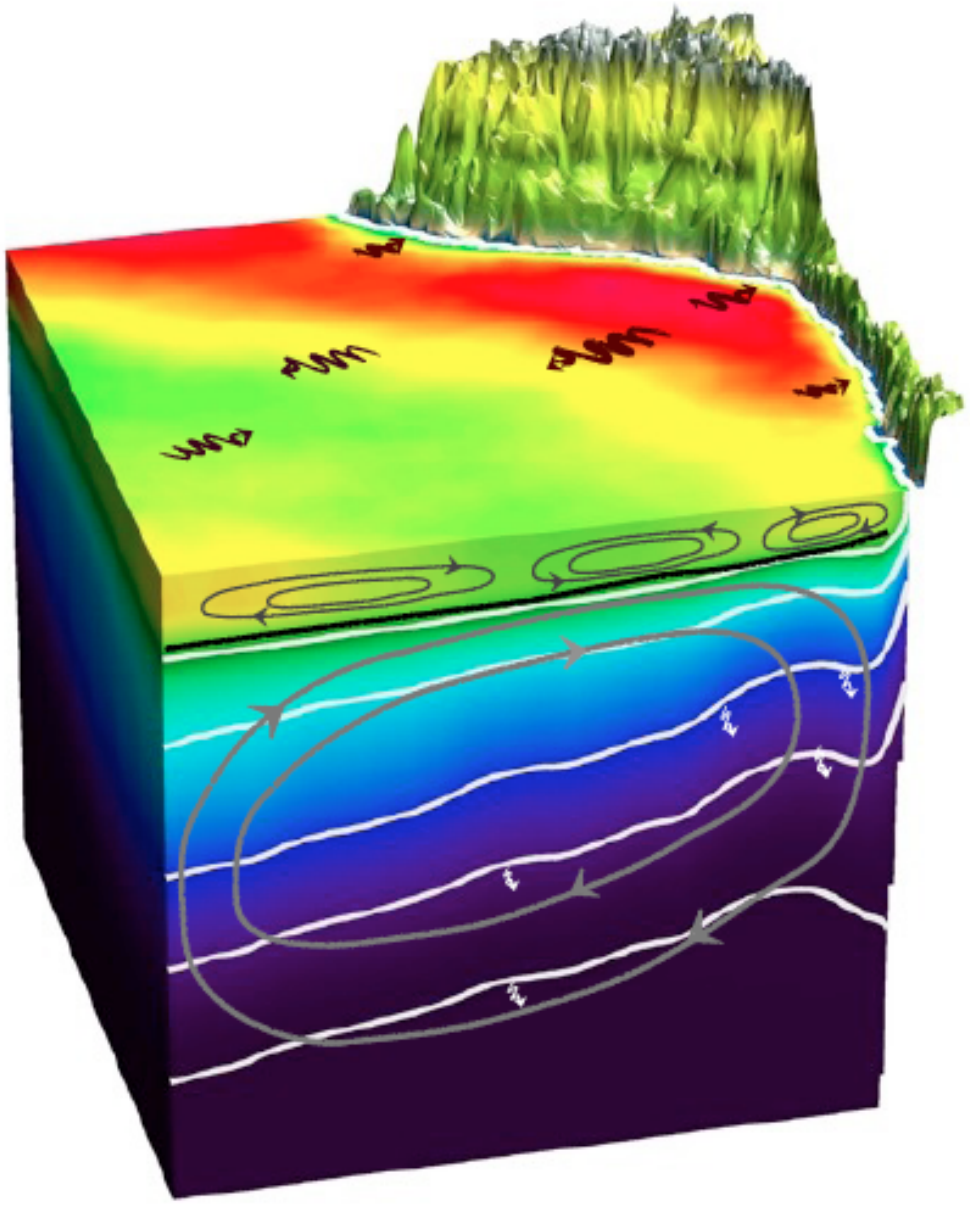

Figure 2: ***3D Schematic representation of the eddy effects on the mean buoyancy field decomposed between adiabatic eddy-induced advection and diabatic/diapycnal flux. (The geometry is for Peru with its Andes mountains.) The mean stratification is indicated by the contours in the foreground vertical plane as well as by the colors. In the surface boundary mixed layer, the adiabatic advective component is associated with the restratication tendency of submesoscale fronts with a lateral scale O(1 km). It is represented by its associated streamfunction (black closed contours in the foreground vertical plane). The diabatic component acts to smooth out surface buoyancy extrema and is shown as sinuous arrows in the top plane. Interior diabatic fluxes represented by white arrows in the foreground vertical plane are found to be negligible in our mesoscale-resolving solutions. Interior adiabatic advective fluxes associated with mesoscale eddies (whose associated streamfunction is shown with gray closed contours in the foreground vertical plane) oppose Ekman-induced transport. Both adiabatic components can be seen as the manifestation of Available Potential Energy release by baroclinic instability and frontogenesis near the surface. (Colas** *et al.***, 2103b)***

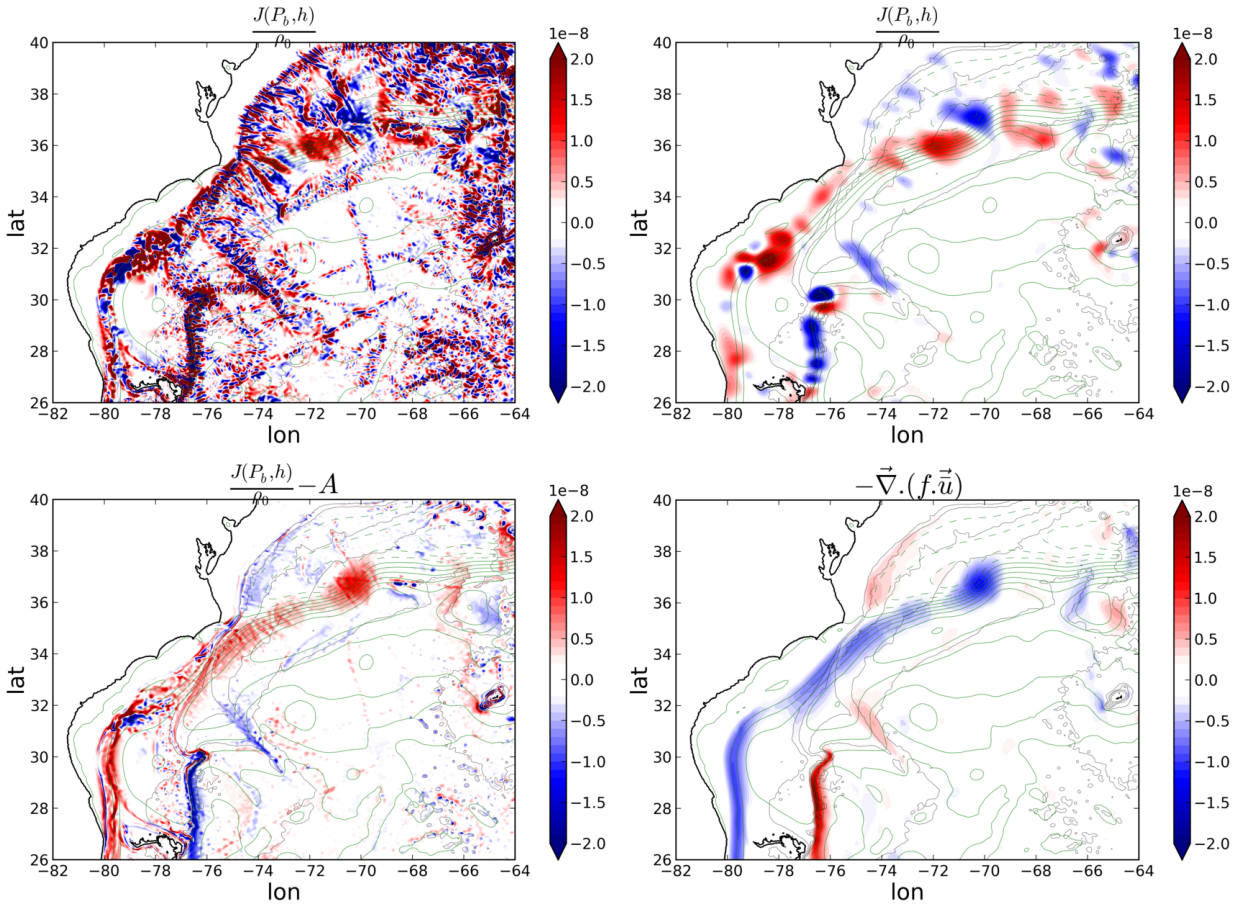

Figure 3: ***Time-mean of (a) Bottom Pressure Torque*** $\frac{J(P_b,h)}{\rho_0}$***, (b) horizontally smoothed Bottom Pressure Torque, (c) sum of the Bottom Pressure Torque and the non-linear advective terms in the barotropic vorticity balance equation*** $\frac{J(P_b,h)}{\rho_0} - A$ ***and (d) the planetary vorticity term*** $-\vec{\nabla}.(f\vec{u})$ ***for 18 years of a*** $2.5km$ ***resolution ROMS simulation. Units are*** $m.s^{-2}$***. Topography is shown in black lines and mean barotropic streamfunction in green lines (contours every 10 Sv).***

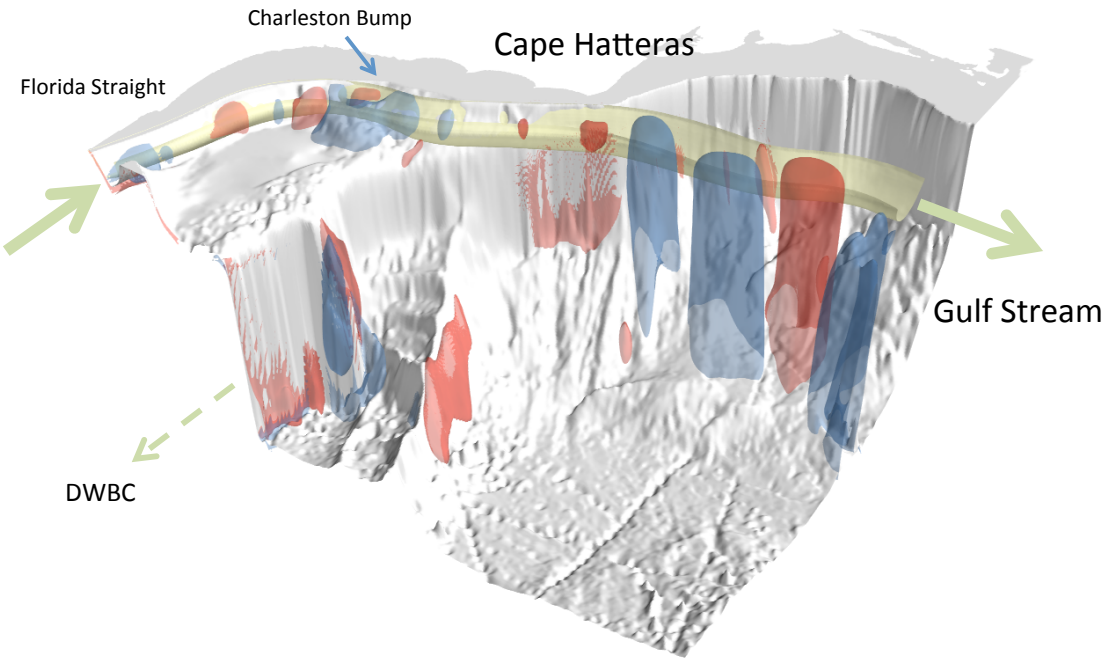

Figure 4: ***Mean vertical advection of absolute vorticity for a 18-year*** $2.5km$ ***resolution ROMS simulation. Blue contour is*** $-0.5e^{-8}ms^{-2}$ ***(downward) and red contour is*** $+0.5e^{-8}ms^{-2}$ ***(upward). The transparent yellow contour shows the path of the Gulf Stream and is defined as*** $\sqrt{u^2+v^2} > 0.5ms^{-1}$***. Strong negative fluxes of vorticity, associated with a southward deflection of the Gulf Steam, are seen at Charleston Bump and after separation of the current from the coast at Cape Hatteras. The deep signals seen at Cape Hatteras and along the Blake Ridge are due to the Deep Western Boundary Current flowing southward and crossing the Gulf Stream path right after its separation.***

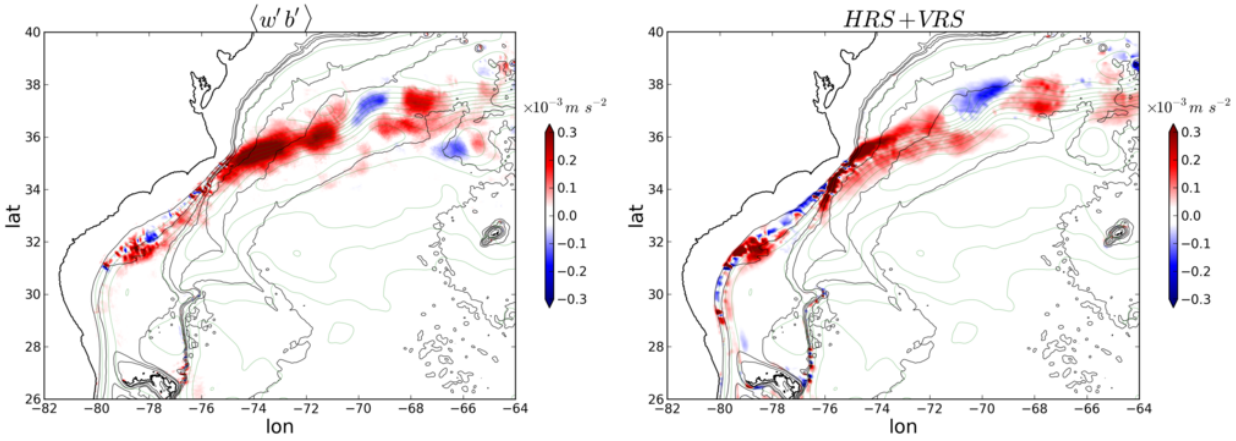

Figure 5: ***Depth integrated eddy potential to eddy kinetic energy conversion*** $P_e K_e = \overline{w'b'}$ ***(*** $m^2.s^{-3}$***) (left) and mean to eddy kinetic energy conversion*** $K_m K_e = HRS + VRS$ ***(*** $m^2.s^{-3}$***) (right) for 18-year*** $2.5km$ ***resolution ROMS simulation. Both energy conversions are at the topographic features, especially the Charleston Bump and at the separation point after Cape Hatteras.***

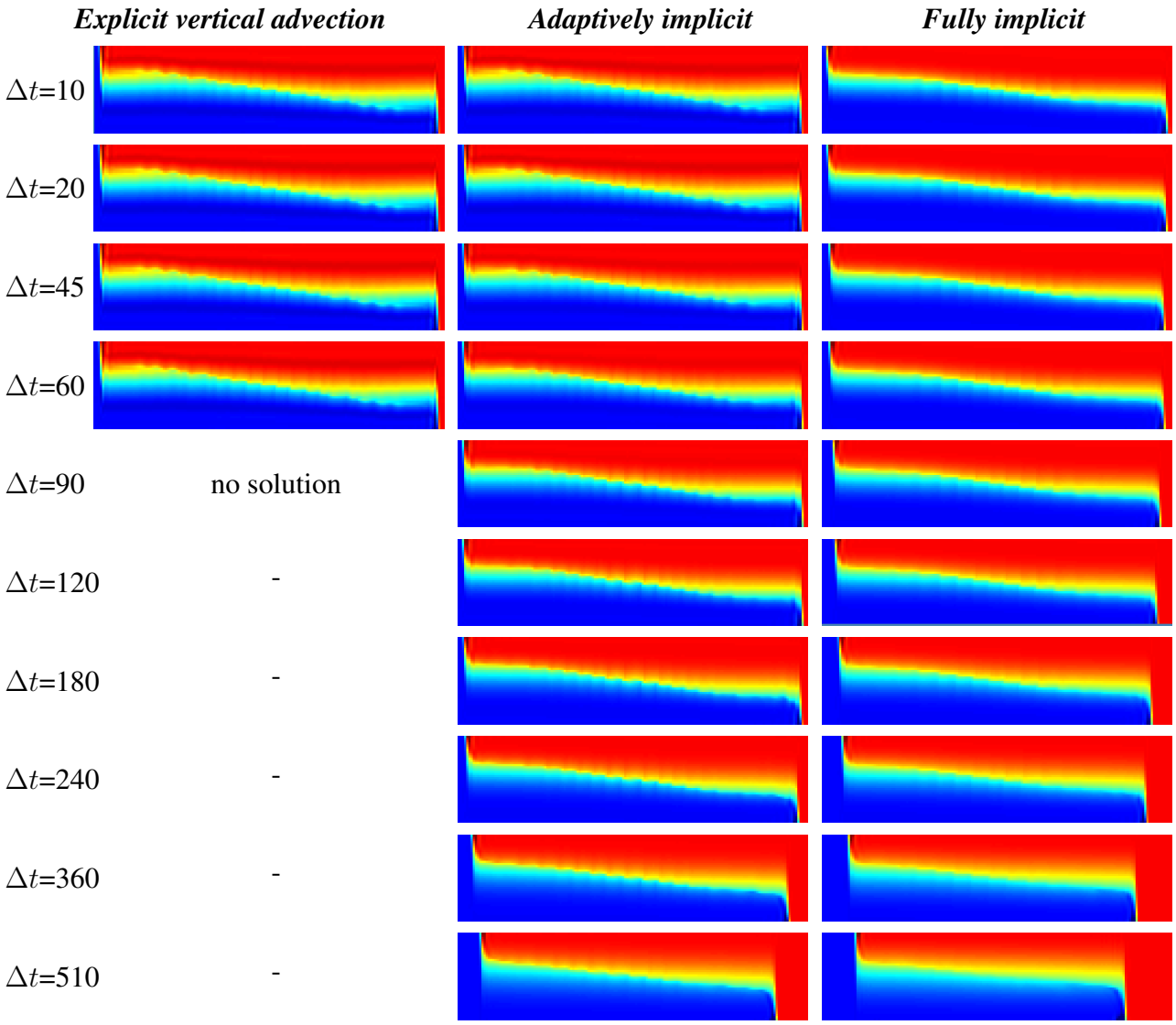

Figure 6: ***Comparison of lock-exchange test solutions using explicit, adaptively implicit, and fully-implicit vertical advection algorithms. The setup is the same as in Ilicak*** *et al.* ***(2012), and it is also a standard ROMS test problem (Haidvogel & Beckmann, 1999) which in its turn, is inspired by the classical work of Benjamin (1968). The solution (vertical along-channel*** xz ***cross-section of temperature field) is shown at 17 hours since initialization which matches Fig. 2 and Fig. 5 from Ilicak*** *et al.* ***(2012). The length of the domain is*** $64km$***, depth is*** $20m$***, grid resolution*** $\Delta x = 400m$***,*** $\Delta z = 0.5m$***. Explicit solution can be obtained for*** $\Delta t \leq 60$***, beyond which the code becomes numerically unstable. Note that vertical-to-horizontal aspect ratios, both*** $\Delta z/\Delta x = 1/800 \ll 1$ ***and*** $h/\Delta x = 1/20 \ll 1$ ***are small, which means that this grid does admit nonhydrostatic effects. Nevertheless, this problem is known to generate sharp fronts with large vertical velocities. Unlike Ilicak*** *et al.* ***(2012) who selected a Smolarkiewicz scheme for tracer advection (the best fit for this particular problem, but is too diffusive for realistic long-term simulations), we use a third-order upstream scheme in the horizontal, and parabolic spline in the vertical (for the explicit part) direction. They also choose to perform their tests with*** $\Delta t = 1s$ ***resulting in vanishingly small CFL, while our goal here is to push it to the limit.***